Downstream Baroclinic Development Among Forty-one Cold-Season Eastern North Pacific Cyclones

Richard E. Danielson*, John R. Gyakum and David N. Straub

Atmospheric and Oceanic Sciences, McGill University, Montréal, Québec

[Original manuscript received 18 March 2004; in revised form 16 July 2004]

ABSTRACT *A quantification of local energy propagation is employed to distinguish cases of downstream baroclinic development, as described by Orlanski and Sheldon (1995), from among 41 cold-season cyclones that intensified strongly over the eastern North Pacific Ocean. A group of western North Pacific cyclones is employed to confirm that, in a composite sense, the eastern group is relatively less dependent on baroclinic conversion and more dependent on eddy energy that originates upstream. Based on a proposed set of criteria, about half of the individual eastern cyclones are found to be good examples of downstream baroclinic development. Almost all of this subset appears to have been influenced by a propagation of eddy energy from separate cyclones developing over the western North Pacific a day or two earlier. A primary source of energy feeding this propagation appears to be ascent in the warm sector of the upstream cyclones.*

RESUMÉ *[Traduit par la rédaction] On utilise une quantification de la propagation de l'énergie locale pour distinguer les cas de développement barocline en aval, tels que décrits par Orlanski et Sheldon (1995), parmi 41 dépressions de saison froide qui se sont fortement intensifiées dans l'est du Pacifique Nord. On emploie un groupe de dépressions de l'ouest du Pacifique Nord pour confirmer que, dans l'ensemble, le groupe de l'est est relativement moins dépendant de la conversion barocline et plus dépendant de l'énergie tourbillonnaire provenant d'en amont. D'après un ensemble de critères proposés, on trouve qu'environ la moitié des différentes dépressions de l'est sont de bons exemples de développement barocline en aval. Presque tout ce sous-groupe paraît avoir été influencé par une propagation d'énergie tourbillonnaire provenant de dépressions distinctes qui s'étaient formées dans l'ouest du Pacifique Nord un jour ou deux auparavant. L'ascendance dans le secteur chaud des dépressions en amont semble être une source principale d'énergie alimentant cette propagation.*

1 Introduction

It has long been appreciated that some extratropical troughs depend on an upstream trough or ridge for their movement and intensification (Namias and Clapp, 1944; Hovmöller, 1949). Comprehensive surveys of waves in the upper troposphere suggest that this dynamical dependence, known as downstream development, occurs throughout the extratropics (Lee and Held, 1993; Chang, 1993; Chang and Yu, 1999). Despite its apparent ubiquity, studies of individual troughs and surface cyclones tend to emphasize a wide variation in the role of downstream development (e.g., Nielsen-Gammon, 1995; Nielsen-Gammon and Lefevre, 1996; Lackmann et al., 1999). The storm track modelling and observational studies of Chang and Orlanski (1993) and Chang (1993) suggest that a dependence on upstream troughs and ridges may be prevalent for cyclones occurring over the eastern North Pacific. Moreover, a climatological maximum in the frequency of strong cyclones in this region (Roebber, 1984) may be attributable in part to downstream development. To understand case-to-case variations in the role of downstream development better, a group of eastern North Pacific cyclones is closely examined.

Modern studies of downstream development have been motivated in part by Simmons and Hoskins (1979) and Orlanski and Katzfey (1991). The former examined linear and non-linear simulations of an initially localized eddy within a zonal baroclinic flow. Focusing on the leading edge of the expanding perturbation flow, Simmons and Hoskins found a cessation of upper-level growth prior to that at the surface, which suggested that eddy energy disperses from predecessor upper-level eddies. They also confirmed that the downstream spread of new disturbances occurs at nearly the speed of the upper-level flow.

Orlanski and Katzfey (1991) diagnosed a southern hemisphere wavetrain, associated with a surface cyclone near Antarctica. They focused on the eddy kinetic energy centres between adjacent trough and ridge axes, and noted that these grow and decay in sequence downstream. Orlanski and

*Corresponding author's e-mail: rick@phys.ocean.dal.ca; current affiliation – Department of Oceanography, Dalhousie University, 1355 Oxford St., Halifax NS B3H 4J1

Katzfey showed that the evolution of the energy centre associated with the surface cyclone is dominated by two processes. Strong ascent in the warm sector of the cyclone defines a baroclinic conversion. This is the largest source of eddy kinetic energy. A net ageostrophic geopotential flux divergence represents the largest sink. This sink also represents an interaction between energy centres: the flux divergence from the cyclone effectively provides a source of eddy energy for the growing ridge immediately downstream.

Orlanski and Katzfey (1991) characterized their event as being weakly forced by topography. However, similar diagnoses were made of an intense cold-air outbreak along the North American west coast (Orlanski and Sheldon, 1993) and the major east coast "Blizzard of 1993" (Orlanski and Sheldon, 1995). These subsequent studies demonstrate that a local eddy energy diagnosis can yield physical insight in a variety of different mid-latitude environments. Even for cases that are strongly forced by orography and diabatic processes, they show that energy dispersion, as measured by the ageostrophic geopotential flux, makes an important contribution to the initial growth and subsequent decay of the energy centres of interest.

Orlanski and Sheldon (1995) reconcile cyclone development as depicted by eddy energy with the more traditional paradigm of a single upper-level trough overtaking a low-level baroclinic zone (Petterssen and Smebye, 1971; Hoskins et al., 1985). They extend this paradigm by emphasizing the role of downstream development, or energy propagation between adjacent troughs and ridges. According to their extended description, which we refer to as *downstream baroclinic development*, eddy kinetic energy west of a ridge axis disperses downstream and initiates energy growth to the west of an incipient trough. Energy growth here, concurrent with a digging trough, occurs initially due to the upstream energy source, and later because of baroclinic conversion (descent in relatively cold air in the wake of a surface cyclone). As this energy centre matures, it becomes an energy source for another centre just east of the trough axis, while the energy centre upstream of the ridge axis decays. Subsequently, the eastern centre is also fed by baroclinic conversion (ascent in relatively warm air ahead of the surface cyclone), and may act as a source of eddy energy for further development downstream.

Although eddy energy that disperses from upstream may be important for the development of some cyclones, it is generally not the only process involved. Nielsen-Gammon (1995) discusses different theories of trough formation in terms of distinct evolutions of potential vorticity. He also examines a particular vorticity maximum over North America which was well observed but poorly forecasted. Downstream development is inferred by the growth of the upstream ridge preceding that of the trough of interest, but this wave also appears to amplify locally by horizontal deformation. Superposition with a lower-frequency wave appears to make a contribution as well. Nielsen-Gammon and Lefevre (1996) further demonstrate that a diagnosis based on potential vorticity can complement a local eddy energy diagnosis. They illustrate that downstream development and baroclinic amplification primarily govern the height tendencies of another trough over North America. However, a barotropic deformation also produces non-negligible intensification at an early stage. Lackmann et al. (1999) note, moreover, that the development of most North American troughs may benefit from barotropic deformation in the presence of a large-scale stationary ridge over western North America. They illustrate this type of development with an east coast cyclone that develops in the absence of energy dispersing across the upstream ridge.

The role of downstream development in particular troughs and surface cyclones may vary widely from case to case, but these variations can be partly attributed to the characteristics of the region or the season in which an event occurs. Lee and Held (1993) and Chang (1999) illustrate the strong tendency for troughs and ridges to organize into wave packets in models and analyses of the southern hemisphere flow. Lee and Held attribute summertime wave packet coherence in this region to the absence of stationary waves and to the weak instability of a zonally confined jet stream, from which small amplitude troughs and ridges tend to develop. They infer that downstream development is occurring because wave packets can remain coherent for many days and because their group velocity is faster than the propagation of individual troughs and ridges. To confirm this, Chang (2000) examines the eddy kinetic energy budgets of a few warm-season wave packets. He finds that the growth and decay of a majority of the individual troughs which define these wave packets can be attributed to an ageostrophic geopotential flux convergence. Chang (2000) also examines strongly intensifying troughs and finds that they show a similar dependence on downstream development.

Although factors inhibiting the coherence of wave packets, such as the presence of stationary waves, are prevalent during the northern hemisphere cold season, the role of downstream development may also be prevalent in localized regions. Chang and Orlanski (1993) address the observation that baroclinicity in the northern hemisphere is generally strongest near the east coast of Asia and North America, although storm tracks are actually more prominent over the mid-latitude oceans (Hoskins and Valdes, 1990). Their idealized simulations successfully reproduce a storm track extension into regions of weak low-level baroclinicity. They prescribe upstream baroclinicity and synoptic-scale perturbations, and allow the downstream region to evolve freely. Under equilibrium conditions, the upstream eddy energy centres grow by baroclinic conversion and decay by ageostrophic geopotential flux divergence. Strong mixing destroys baroclinicity, but near the downstream end of the model domain, the weaker baroclinicity does not correspond to a decaying storm track because the growth of these downstream energy centres is aided by eddy energy propagation from upstream.

Observational support for Chang and Orlanski (1993) was provided by Chang (1993) and more recently by Hakim (2003). The former study uses lagged regression to calculate an eddy energy budget for cold-season synoptic-scale waves. This shows a downstream ageostrophic geopotential flux between composite eddy kinetic energy centres. Budget results

at different time lags also reveal that the importance of baroclinic conversion decreases, and energy dispersion increases, in moving from west to east across the North Pacific Ocean. The latter study examines downstream wave packet evolution following surface cyclone development at the entrance to the North Pacific storm track. Favourable comparisons are made between observed and theoretical evolutions. Hakim (2003) also indicates that western North Pacific cyclones may be precursors of subsequent cyclones much farther downstream.

Cyclones are generally the result of a variety of interacting processes and prior studies that have examined eastern North Pacific cyclones have invariably emphasized low-level baroclinicity. Roebber (1984) speculated that in the absence of strong sea surface temperature gradients, such an environment could be provided by outbreaks of Arctic air through the Bering Strait. This would be consistent with cases that form in the wake of a decaying cyclone in the Gulf of Alaska. Reed and Albright (1986) emphasize the baroclinic forcing of a particularly intense event, as well as the role of preconditioning surface heat fluxes, weak static stability, and an extended period of warm moist inflow in the warm sector. Numerical simulations of the same case by Reed and Albright (1986) confirm a strong sensitivity to the inclusion of moist processes. These studies also emphasize the detrimental effect on analyses of a lack of observations in this region, but their focus is mainly on local sources of energy.

Cyclone climatologies have so far provided the bulk of the evidence that eastern North Pacific cyclones benefit in part from downstream development. It may also be relevant that during the northern hemisphere cold season, extratropical waves are associated with wavelengths of about 4000 km (Wallace et al., 1988) and with wavenumbers of six or seven (Chang and Yu, 1999), corresponding to a little over two waves across the North Pacific Ocean. Some surface climatologies are suggestive of a local maximum in strong cyclogenesis in the eastern North Pacific (e.g., Sanders and Gyakum, 1980; Murty et al., 1983; Roebber, 1984). This could be interpreted as resulting from the primary maximum in cyclogenesis in the western North Pacific (Gyakum et al., 1989). Such an interpretation would thus depend on a systematic propagation of energy across developing ridges in the mid-North Pacific toward predecessor upper-level troughs. It is also possible, however, that the intensity of some eastern cyclones are simply discovered once they track into a region of better observational coverage (cf. Roebber, 1984).

For a group of strong eastern North Pacific cyclones, this study proposes a quantitative means to identify good examples of downstream baroclinic development (Orlanski and Sheldon, 1995). The upstream sources of eddy energy dispersion are also identified. Section 3 describes the eddy energy budget and our selection of events. Composite aspects of the cyclones of interest are provided in Section 4 and all events are briefly characterized according to our downstream baroclinic development criteria in Section 5. The application of these criteria to a few examples is illustrated in Section 6, followed by a summary in Section 7. The next section describes the datasets employed.

2 Data

Surface cyclones are chosen from a comprehensive database of events which occurred over the North Pacific Ocean during ten consecutive six-month cold seasons (1 October – 31 March; 1975/76 – 1984/85). Cyclones have been identified as sea level pressure minima surrounded by at least one closed isobar (using a 4-hPa contour interval). Their central pressures and positions have been tabulated at 00:00 UTC and 12:00 UTC based on the six-hourly final northern hemisphere manual sea level pressure analyses produced by the United States National Centers for Environmental Prediction (NCEP). A surface cyclone climatology based on events from the first eight seasons of this dataset is described by Gyakum et al. (1989).

We employ a conventional measure of cyclone intensification, which is the 24-h central pressure change (in hPa $[24\text{-h}]^{-1}$) normalized by $(24 \times \sin \varphi_m / \sin 60°)$, where φ_m is the cyclone's mean latitude. Normalization accounts for the latitudinal variation in geostrophic wind, and the result is expressed in units of Bergerons (Sanders and Gyakum, 1980). Although special effort was used by NCEP analysts to resolve the position and central pressure of individual surface cyclones (Corfidi and Comba, 1989), the sparsity of North Pacific observations has likely led to some poorly documented developments in both the subjective and objective analyses employed herein.

Gridded objective analyses used to compute energy budgets are the NCEP/National Center for Atmospheric Research (NCAR) global reanalyses (Kalnay et al., 1996) at 2.5° latitude–longitude resolution and on 17 pressure levels. These data include horizontal wind components, pressure vertical velocity, geopotential height, temperature, as well as surface and sea level pressure. Prognostic variables used by the hydrostatic data assimilation system are vorticity, divergence, virtual temperature, specific humidity, and surface pressure. In post-processing the 6-hourly analyses, wind components are computed and the resulting variables are interpolated from a spectral representation to spherical coordinates. Geopotential height and vertical velocity are derived, and an interpolation is performed from the 28 model sigma levels to pressure levels. Some variables (e.g., horizontal and vertical motion, temperature, and geopotential height) have also undergone a spectral smoothing. Observations assimilated by the NCEP/NCAR reanalysis include sea level pressure over the oceans.

3 Methodology

a *Case Selection*

The 50 most strongly deepening cyclones from 10 cold seasons are identified using a domain of 20°N to 70°N and 170°W to 120°W, which encompasses the long-term regional maximum in intensification (Gyakum et al., 1989). We focus on strong cyclones in part because their onset of maximum 24-h deepening provides a robust temporal point of reference. Six pairs of these events deepen within five days of each other and this is undesirable for statistical purposes. Thus, one of each pair is excluded (the one that maximizes the time between remaining events), leaving 44 events.

Along with a temporal reference, we also consider a common spatial point of reference. One obvious candidate is the position of the surface cyclone itself, although a more relevant position in terms of downstream baroclinic development is the position of the associated upper-level trough. Morgan and Nielsen-Gammon (1998) demonstrate the utility of an "isertelic'' analysis, which is defined on a surface of constant Ertel potential vorticity at a level representative of the dynamic tropopause. This field captures the dynamically relevant upper-level features at a single level, with troughs corresponding to either potential temperature minima or pressure maxima (tropopause depressions hereafter). In constructing this analysis, we use the hydrostatic approximation of potential vorticity (*PV*), defined in pressure and spherical coordinates (Hoskins et al., 1985) as

$$PV = -\frac{g}{a\cos\varphi}\left(\frac{\partial V}{\partial\lambda} - \frac{\partial U\cos\varphi}{\partial\varphi}\right)\frac{\partial\Theta}{\partial p} - gf\frac{\partial\Theta}{\partial p} - \frac{g}{a}\frac{\partial\Theta}{\partial\varphi}\frac{\partial U}{\partial p} + \frac{g}{a\cos\varphi}\frac{\partial\Theta}{\partial\lambda}\frac{\partial V}{\partial p}. \quad (1)$$

Here, g is the constant of gravity, a is the mean radius of the earth, Θ is potential temperature, f is the Coriolis parameter, and U and V are the zonal and meridional winds, respectively. The longitude, latitude, and pressure coordinate system is denoted by λ, φ, and p, respectively. Computation of *PV* is made by centred differences, but vertical derivatives are first calculated at mid-levels between the data levels, then interpolated linearly in pressure from mid-levels to the original data levels. We take the dynamic tropopause as the 2-PV unit surface (a PV unit is defined as $10^{-6}\mathrm{m}^2\ \mathrm{s}^{-1}\ \mathrm{K\ kg}^{-1}$).

Tropopause depressions are subjectively tracked at the resolution of the gridded analyses. Of the 44 cyclones of interest, another three cases are excluded because they are not associated with a mobile tropopause depression that can be tracked for over five days centred on the onset of maximum surface deepening. (One of these cases was documented by Reed and Albright (1986), who also had difficulty in tracking the upper-level short wave through a stationary ridge upstream.) The evolution of the remaining 41 events is discussed below.

b *Energy Budget Equations*

Following Orlanski and Katzfey (1991), downstream baroclinic development is described in the context of the eddy kinetic energy budget. Here, a quasi-Lagrangian, rather than Eulerian, form is considered. Terms are computed following the motion of each tropopause depression to facilitate averaging over all cases of interest. For a domain moving horizontally with velocity $\mathbf{C}$, the quasi-Lagrangian tendency is

$$\frac{\delta}{\delta t} = \frac{\partial}{\partial t} + \mathbf{C}\cdot\boldsymbol{\nabla}_p, \quad (2)$$

where $=_p$ is the two-dimensional gradient operator on a constant pressure surface. Denoting eddy variables with the lower case and 30–day mean variables with an overbar, the horizontal wind velocity, three-dimensional wind velocity, and geopotential height are

$$\begin{aligned} \mathbf{V} &= (U, V, 0) = \overline{\mathbf{V}} + \mathbf{v}, \\ \mathbf{U} &= (U, V, \omega) = \overline{\mathbf{U}} + \mathbf{u}, \\ \Phi &= \overline{\Phi} + \phi, \end{aligned} \quad (3)$$

respectively. The budget of eddy kinetic energy per unit mass $\left(K_e = \frac{1}{2}u^2 + \frac{1}{2}v^2\right)$ is

$$\frac{\delta}{\delta t}K_e = -\nabla_p\cdot K_e(\mathbf{V}-\mathbf{C}) - \frac{\partial}{\partial p}\left(K_e\omega\right) - \mathbf{v}\cdot\nabla_p\phi - \mathbf{v}\cdot\left(\mathbf{u}\cdot\nabla\overline{\mathbf{V}}\right) + \mathbf{v}\cdot\overline{\left(\mathbf{u}\cdot\nabla\mathbf{v}\right)} + R. \quad (4)$$

We take the 30-day time mean to be centred on the onset of surface deepening. Prior case studies have used a spatial mean or a longer time mean (Orlanski and Sheldon, 1993; Lackmann et al., 1999), although a 30-day time mean appears adequate to capture the spectrum of wave frequencies relevant to downstream development (Chang and Yu, 1999).

The left-hand side term in Eq. (4) represents a local storage of kinetic energy in a domain following the tropopause depressions. The first two right-hand side terms are the horizontal and vertical components of quasi-Lagrangian flux convergence and represent a net import of energy into the moving domain. The third term is called the generation term and represents work done by the pressure gradient force in cross-isobaric flow. The next term is the Reynolds' stress, which is related to a corresponding term in the mean kinetic energy budget. Hence its interpretation is that of a contribution to mean-eddy transfer (Orlanski and Katzfey, 1991). The second to last term can also be interpreted as a transfer between different forms of kinetic energy, though it is identically zero in an averaged sense. The final term in Eq. (4) is the budget residual representing energy dissipation and discretization errors. Formally, it also contains a term associated with the non-steadiness of the mean flow, but this is negligible in practice.

For a non-divergent time-mean flow, the eddy generation term can be expressed as

$$-\mathbf{v}\cdot\boldsymbol{\nabla}_p\phi = -\boldsymbol{\nabla}_p\cdot\left(\phi\mathbf{v}\right)_a - \frac{\partial}{\partial p}\phi\omega - \alpha\omega \quad (5)$$

where the term involving eddy specific volume (α) represents a conversion from eddy available potential to kinetic energy. We refer to the $(\phi v)_a$ term as the ageostrophic geopotential flux, which is defined as

$$\left(\phi \mathbf{v}\right)_a = \phi \mathbf{v} - \hat{\mathbf{k}} \times \nabla \frac{\phi^2}{2f} \tag{6}$$

where $\hat{\mathbf{k}}$ is a unit vertical vector. Note that this flux differs slightly from the geopotential multiplied by the ageostrophic wind, owing to the variable Coriolis parameter. Following Orlanski and Sheldon (1993) and Chang and Orlanski (1994), this is the eddy geopotential flux with the non-divergent (essentially geostrophic) part omitted.

To highlight the lateral direction of energy propagation that is characteristic of downstream development, local quantities are vertically integrated. This results in a simplification of the local budgets insofar as the interactions between adjacent eddy kinetic energy centres are emphasized (cf. Orlanski and Sheldon, 1993) and the vertical flux convergence terms in Eq. (4) and Eq. (5) become quite small. Integrals are performed from the surface to 100 hPa (the upper limit of the vertical velocity data), normalized by the constant of gravity to obtain units of J m^{-2} for energy and W m^{-2} for the budget terms.

Given a single vertically integrated eddy kinetic energy centre and its budget terms, a concise summary is obtained by integrating over an appropriate area. However, such a budget summary generally depends on the boundaries of this area. Following Orlanski and Sheldon (1995), we employ an energy contour that delimits the centre. This has the advantage of emphasizing the role of source and sink terms over advective terms, although it generally requires a subjective procedure to isolate the energy centres of interest. The procedure employed here involves first finding all local maxima and the regions around these for which energy decreases monotonically. (For any gridbox claimed by two maxima, the larger of the two energy maxima divided by the distance to the gridbox in question is considered the "owner''.) This procedure conveniently divides into regions the vertically integrated eddy kinetic energy, and permits a subjective tracking (corresponding to that of the tropopause depressions) of any given energy centre using the appropriate region or group of regions.

Energy centres adjacent to a tropopause depression are typically easy to isolate using the above method. Energy centres farther upstream are identified by whether there is an ageostrophic geopotential flux from them toward the tropopause depression of interest. We define all energy centres by a cutoff energy contour of 0.75 MJ m^{-2}. (This is slightly more inclusive, but nearly equivalent to the 100 m^2 s^{-2} vertically averaged contour used in previous studies.) A few of these regions are shown in Section 6 to demonstrate that they are well defined. Because the amplitude of the energy centres (and their budget terms) varies in time and from case to case, we compute growth rates at each time by normalizing each volume integrated budget term by the volume integrated eddy kinetic energy. Growth rates thus defined are reasonably robust to various choices of the cutoff contour.

4 Group characteristics

Although important case-to-case variations are masked, it is convenient to introduce the evolution of the eastern North Pacific cyclones in an averaged sense. Following Chang (1993), this approach permits us to examine whether eastern cyclones tend to benefit from a downstream propagation of eddy energy, and whether baroclinic conversion is weak relative to that of western North Pacific cyclones. Most of the eastern cyclones deepen rapidly shortly after they form. While deepening, they move over a relatively weak composite sea surface temperature gradient (Fig. 1). Cases follow a generally cyclonic trajectory toward Alaska, consistent with a large-scale steering flow defined by a decaying cyclone near the Aleutian Islands. Indeed, such a decaying cyclone is present in nearly half of our events (not shown) and may have augmented deepening rates because it defines an environmental pressure gradient down which certain cases tracked. According to the manual analyses, the average deepening rate for this group is 1.5 Bergerons with a standard deviation of 0.3 Bergerons. According to the more objective NCEP/NCAR reanalysis sea level pressure (SLP) fields, the average intensification is 1.1 Bergerons with a standard deviation of 0.3 Bergerons.

Associated with each surface cyclone is a tropopause depression (the individual tracks are shown in Fig. 5). We have averaged the positions of these upper-level features relative to the onset of maximum surface deepening (T0 hereafter) to obtain the composite track shown in Fig. 1. The average tropopause depression is slightly upstream of most surface cyclones at T0, and is found downstream of most cases a few days later. Averages of the individual tropopause depression phase speeds indicate a peak of 18 m s^{-1} at about T0, and a five-day average speed of 15 m s^{-1}, which is slightly faster than corresponding phase speeds estimated by Chang and Yu (1999) and Hakim (2003), but slower than their estimates for energy propagation. As surface cyclones intensify, the average tropopause depression pressure increases by about 25 hPa to values of 430 hPa over 2.5 days.

Composite evolutions of SLP, 500-hPa vertical velocity, and vertically integrated eddy kinetic energy are constructed using the mobile tropopause depressions, rather than geography, as a common spatial reference (Fig. 2). Ascent (dashed contours) is found downstream and descent upstream of the tropopause depressions. The composite surface cyclone of interest is most easily located at T0+24 h, when it is just north of the composite tropopause depression (Fig. 2c). Prior to this time, the predecessor cyclone in the Gulf of Alaska, with ascent to its north-east, is more apparent. As the cyclones of interest become the dominant surface features in this region, the average of their central pressures is about 970 hPa and they begin to fill (not shown). This coincides with an average relative vorticity peak of 4.6×10^{-4} s^{-1}, followed by a spin down. Presumably, this early onset of decay is related to the proximity of orography downstream, which may have impeded the movement of some surface cyclones while the associated tropopause depressions continued to propagate downstream (Martin et al., 2001).

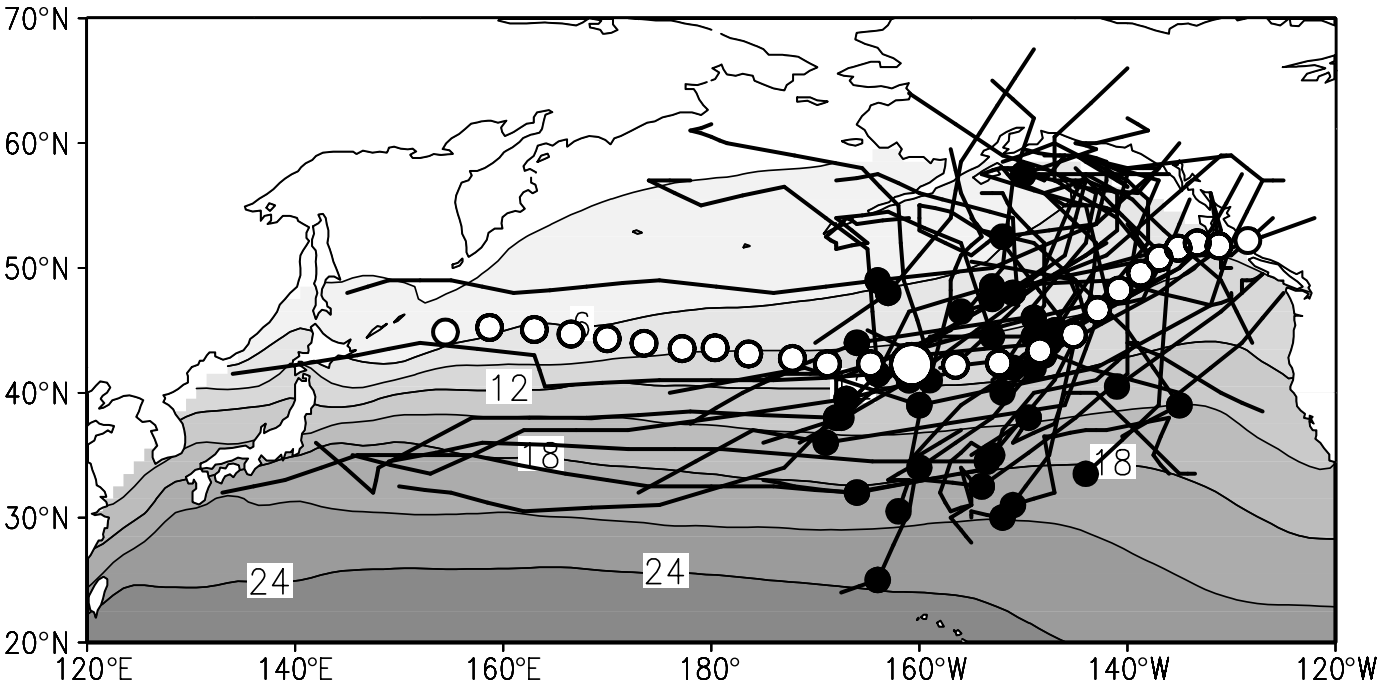

Fig. 1 Subjectively analysed cyclone tracks and composite sea surface temperature (shaded at 3°C intervals; individual sea surface temperature fields are computed from available surface observations following Gyakum and Danielson (2000)). Closed circles indicate position at T0. Open circles show the composite track of the tropopause depressions (the large open circle indicates position at T0).

Eddy energy centres adjacent to our tropopause depressions evolve in sequence, which is consistent with downstream development. The energy centre just upstream grows until T0. It then decays, during which time the downstream centre more than doubles in strength. Ageostrophic geopotential fluxes maximize near the trough axis, which contributes to the decay of the upstream energy centre and growth of the downstream centre, as inferred from Eq. (5). The decay stage following rapid surface deepening is marked by cyclonic circulation of this flux about the tropopause depression. Orlanski and Sheldon (1995) associate this with upper-level wave breaking, which is typically characterized by an overturning tropopause potential temperature contour (Thorncroft and et al., 1993; Magnusdottir and Haynes, 1996; Martin et al., 2001). By the latter definition, wave breaking is associated with 15, 18, and 34 tropopause depressions at T0-24 h, T0, and T0+24 h, respectively (not shown). Following T0, energy also disperses across the developing ridge downstream.

The importance of energy propagation as a possible source of eddy kinetic energy for these eastern cyclones can be demonstrated by comparison with a similar group of 41 western North Pacific cyclones. We have chosen a group whose maximum deepening rates match those of our eastern cases. (If cyclone intensity change is measured by changes in wind speed or vorticity, then the deepening rate can be ambiguous because it does not account for changes in the environmental pressure field. However, we have computed 24-h growth rates following Gyakum and Stewart (1996) and find similar averages of $(1.2\ \mathrm{d})^{-1}$ and $(1.4\ \mathrm{d})^{-1}$ for the eastern and western groups, respectively.) Only one western cyclone occurs immediately upstream of an eastern cyclone. Hence, the eastern and western events are well separated in time and appear unrelated. Composite evolutions of vertically integrated baroclinic conversion and ageostrophic geopotential flux are shown in Fig. 3. Baroclinic conversion occurs upstream of the eastern tropopause depressions until T0, and downstream of the western tropopause depressions from T0 onward. It is possible that the downstream differences are attributable not just to the baroclinicity of the mean flow being stronger in the western North Pacific, but also to differences in eddy heat fluxes and in diabatic processes (all three factors might benefit the western group more, although an examination of the eddy available potential energy budget is beyond our present scope).

Baroclinic conversion is most prominent upstream of the eastern group at T0-24 h (Fig. 3d). Descent of relatively cool air corresponds to a baroclinic conversion just upstream of the eastern tropopause depressions (Fig. 2a). Farther upstream, baroclinic conversion is associated with ascent in the warm sector of certain upstream cyclones. Such a generation of eddy kinetic energy is normally accompanied by ageostrophic geopotential flux divergence, and energy dispersing across the upstream ridge and toward the tropopause depressions is indeed apparent in Figs 3d and 3e (for clarity, only every other vector is plotted and fluxes less than 7 MW m^{-1} are not shown). These results are thus consistent with Chang and Orlanski (1993) and Chang (1993)

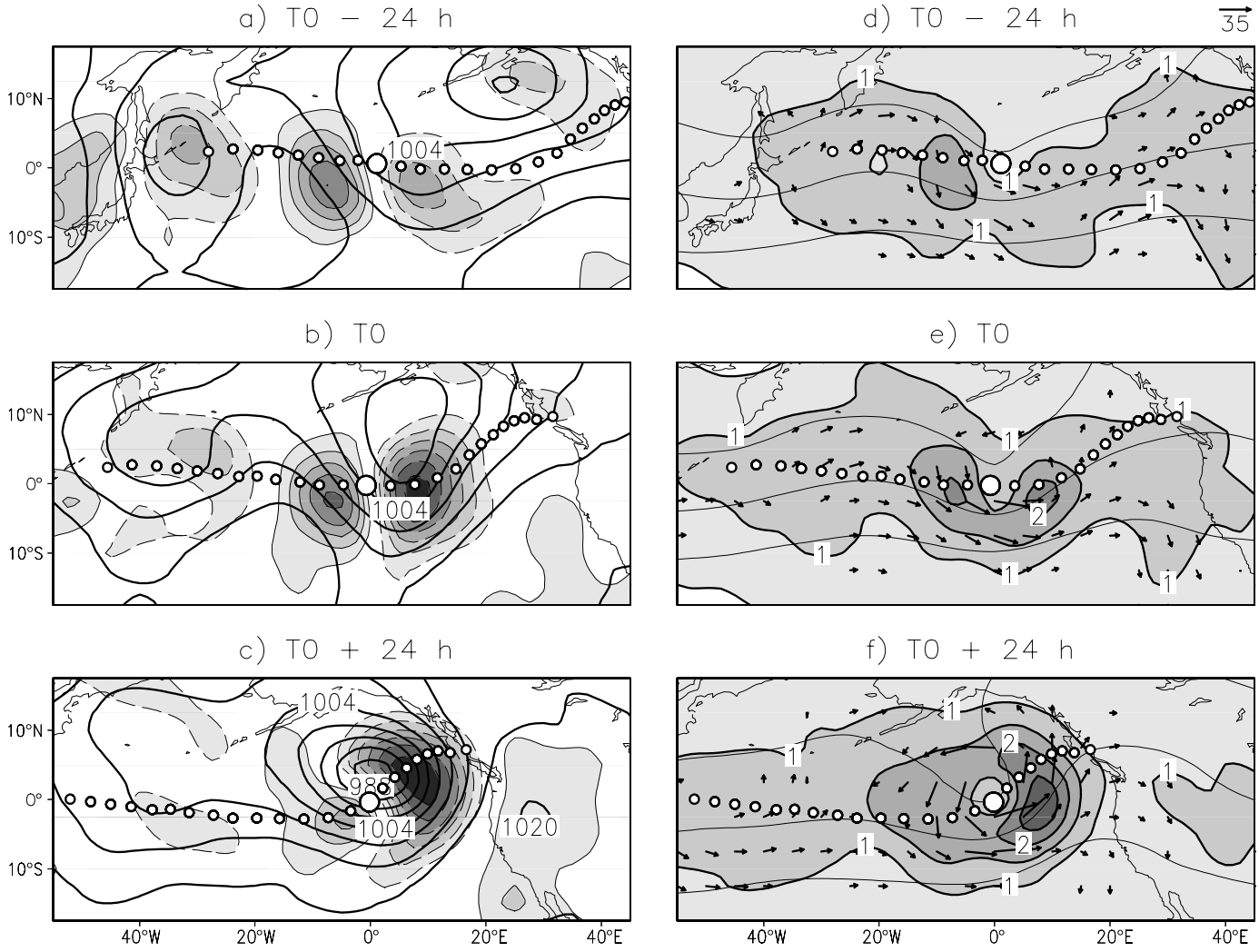

Fig. 2 Composite fields at different times relative to T0: a–c) thick contours show sea level pressure at 4-hPa intervals, and shading indicates the 500-hPa vertical velocity at 0.05–Pa s^{-1} intervals with dashed contours corresponding to upward motion; d–f) vertical integrals of eddy kinetic energy (shaded at 0.5–MJ m^{-2} intervals), ageostrophic geopotential flux (vectors less than 7 MW m^{-1} are omitted), and 500-hPa height (20-dam intervals). As with subsequent figures, geography is shown relative to the position of the tropopause depression track.

insofar as an energy propagation may preferentially support the development of eastern cyclones.

5 Development criteria

While downstream baroclinic development appears more relevant in the eastern North Pacific than in the western, we might expect each of the 41 eastern cyclones to differ somewhat from their composite evolution. In this section, we propose a quantitative set of criteria based on eddy energy in order to identify individual examples of downstream baroclinic development. Firstly, we note that individual evolutions can generally be treated with respect to three vertically integrated eddy energy centres, whose sequential evolutions are summarized below. Specifically, the energy centre that is collocated with the eastern surface cyclone of interest and is just downstream of the eastern trough is referred to as the *eastern* energy centre. The *central* energy centre is between the eastern trough and an upstream ridge and the *western* energy centre is just upstream of this ridge. Individual evolutions are thus summarized in terms of these energy centres, which form a wavetrain when they are all present.

To identify cyclones that were likely to have been influenced by a propagation of energy from upstream, we stipulate that:

- Prior to the intensification of each surface cyclone, an ageostrophic geopotential flux should first be found from the western energy centre toward the central energy centre.
- A subsequent period of time should exist during which eddy energy that disperses toward the central energy centre provides the most important contribution to the growth of this centre, with the possible exception of an in situ baroclinic conversion.
- The previous criterion is then applied to the eastern energy centre.

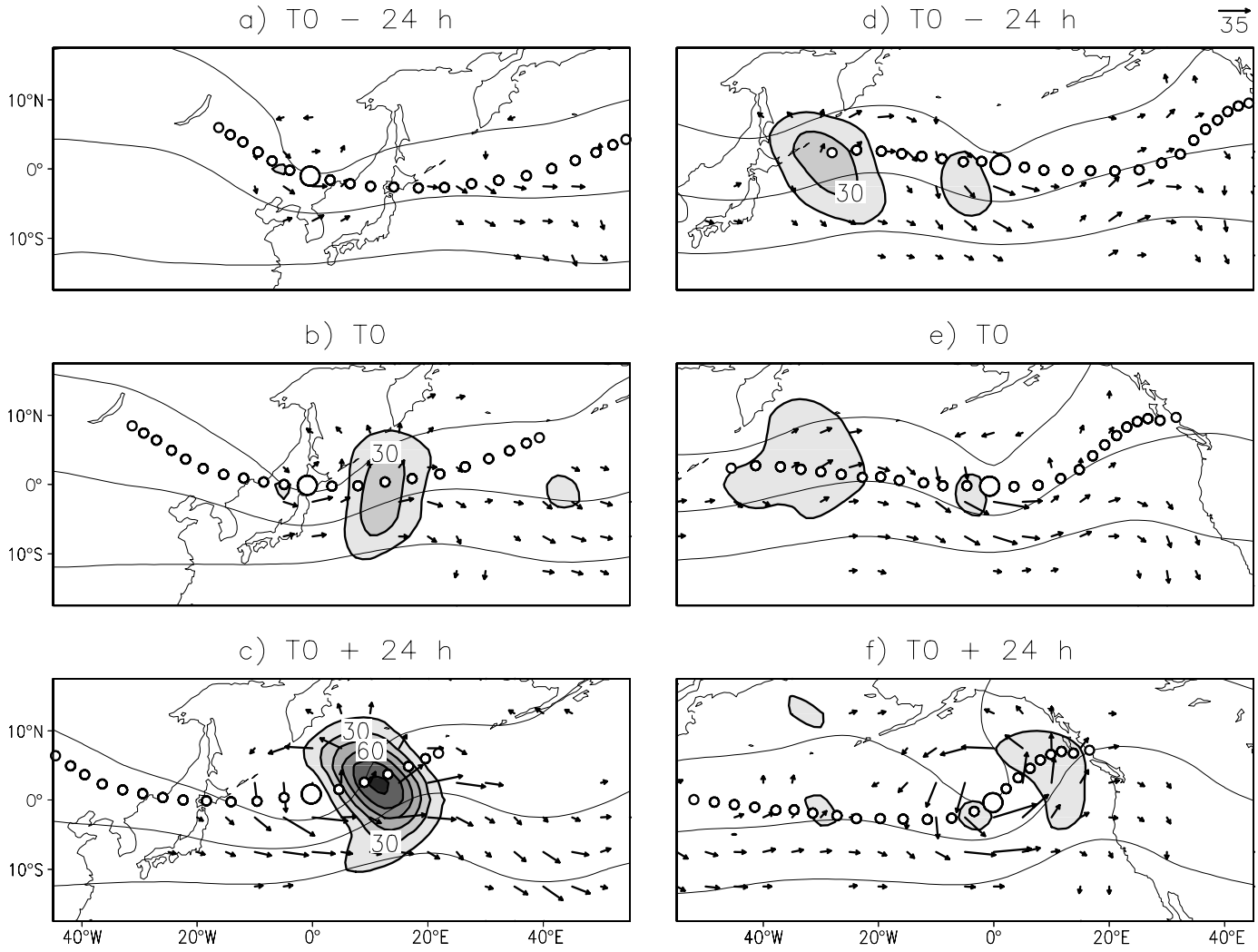

Fig. 3 Composites of the vertically integrated eddy baroclinic conversion term (shaded at 15–W m^{-2} intervals). Also shown are the ageostrophic geopotential flux and 500-hPa height (contour intervals as in Fig. 2). a–c) Western cyclone group. d–f) Eastern cyclone group (see text for further details).

In other words, eddy energy dispersing from the western energy centre should first contribute to the growth of an intermediate energy centre. This intermediate centre is about half a wavelength upstream of the incipient eastern surface cyclone and is typically collocated with a region of descent (Fig. 2). Eddy energy that disperses from the intermediate centre should then contribute to the growth of the eastern energy centre, which is collocated with ascent and the eastern cyclone. We also allow for dominant contributions by baroclinic conversion owing to our focus on eastern cyclones whose surface development is strong by definition. The first criterion is verified by inspection, and instantaneous growth rates averaged over appropriate 24-h periods are used to quantify the latter two criteria. Averaging over 24 h is expected to highlight processes that are important over this period, and should be more robust than an instantaneous growth rate.

To measure the importance of energy dispersing toward an energy centre, we consider only the *positive* contribution of the ageostrophic geopotential flux convergence term within the centre. This contribution is assumed to result from the flux from an upstream energy centre (and the negative contribution is due to a flux toward a downstream energy centre). Typically, this is reasonable before strong non-linearities begin to develop at T0 and at upper levels. The justification for this is based mainly on the central and eastern energy centres of Cases 8, 10, 12, 15, 24, 29, 33, 39, and 41 (where case numbers are taken from Tables 1 and 2), which mature quickly insofar as they disperse nearly equivalent amounts of energy downstream as they receive from upstream. In these cases, the growth and decay phases of the individual centres are difficult to distinguish, and the importance of an initial baroclinic conversion upstream necessarily becomes obscure. When the idealized phases of ageostrophic geopotential flux convergence, followed by baroclinic conversion, and then flux divergence are more apparent, it is possible to modify our criteria to employ the full flux convergence term rather than just the positive contribution. However, this particular

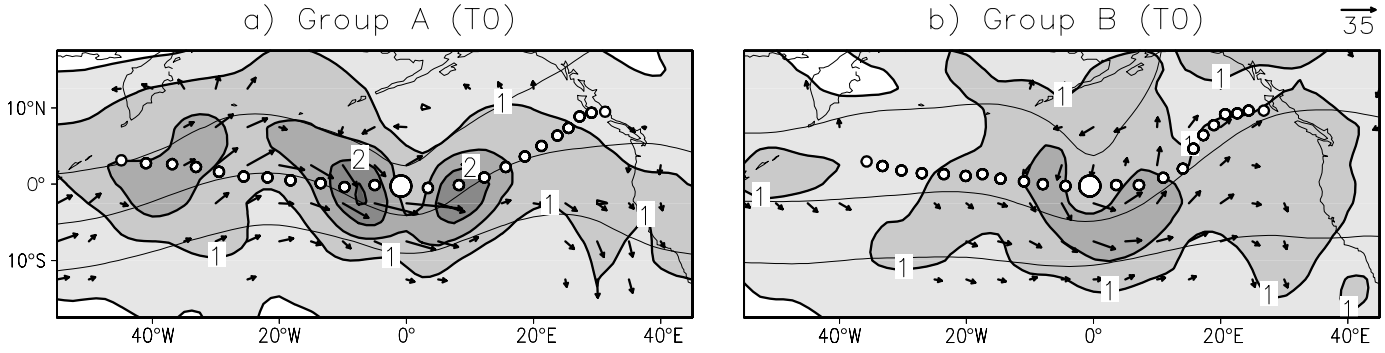

Fig. 4 Composite vertically integrated eddy kinetic energy as in Fig. 2e, but for a) the 20 eastern North Pacific cyclones that meet our criteria for downstream baroclinic development and b) the 21 cyclones not meeting these criteria.

aspect of the idealized evolution does not seem to hold for many eastern North Pacific events that we examine. It is not surprising, moreover, that some evolutions are complex near the end of the North Pacific storm track (e.g., the eastern energy centre of Case 24 grows and decays twice in about four days).

Of the 41 eastern cyclones of interest, 20 meet our proposed downstream baroclinic development criteria and 21 do not. We refer to the former as Group A and the latter as Group B. To demonstrate that our criteria help to distinguish cases which dominate the composite evolution of Section 4, we briefly examine the composite eddy energy and ageostrophic geopotential fluxes of these two groups (Fig. 4). As with the composite of all 41 events (Fig. 2e), important case-to-case variations are masked. However, whereas a western energy centre is clearly evident for Group A, no such centre is seen for Group B. Consistent with this are the dispersive energy fluxes upstream which are apparent only for Group A. By contrast, Group B appears to be characterized by a zonal flow upstream, although a number of undular flows are also included in this group (Fig. 5). Farther downstream, the cyclonic circulation of eddy energy about the Group–B tropopause depressions (Fig. 4b) is consistent with a slight preference for early wave breaking among these events, as 11 of the 18 wave breaking events noted in the previous section are Group–B events.

A summary of the individual Group A evolutions is given in Table 1. By examining cases separately, we can identify the upstream sources of eddy energy propagation. These are almost always the energy centres associated with western cyclones at various stages in their development. The maximum deepening rates of these extratropical cyclones indicate neither that these precursors are particularly intense events (perhaps with the exception of the extratropical decay of super typhoon Tip), nor that their period of maximum intensification is well synchronized with the evolution of interest. The positions of these western cyclones are shown in Fig. 5 by open circles.

Baroclinic conversion is generally positive among the western energy centres of Group A. The ageostrophic geopotential flux convergence term is usually negative, but because baroclinic conversion tends to be larger, most of the western energy centres grow as they disperse energy downstream. About 24 h later, positive contributions from energy dispersing toward the central centres are on the order of $(1\ d)^{-1}$. By criterion 2, this is larger than any of the other contributions besides baroclinic conversion (though this is larger only for Cases 6, 15, 30, 32, and 34). The net growth of the central energy centre by ageostrophic geopotential flux convergence is not very large due to the negative contributions made by this term. Another 24 h later or so, there is typically a net flux convergence in the eastern centre, along with a baroclinic conversion. (In some cases, energy that disperses farther downstream results in a net negative contribution, as in Case 8.) By criterion 3, the positive contributions from energy dispersion are largest during this period (again, except in Cases 8 and 20 where this is second only to baroclinic conversion).

Among the western energy centres of Group B, many are also associated with a western surface cyclone (Table 2). However, the period of strongest surface intensification seems poorly synchronized in comparison to Group A events (i.e., very early in Cases 19 and 31, and late in Cases 1, 7, 11, and 40). Furthermore, baroclinic conversion is not always strong for the western energy centre, though energy dispersing toward eastern troughs is sometimes robust. Criterion 2 is not usually satisfied by this group, since Reynolds' stresses, quasi–Lagrangian flux convergence, and eddy forcing terms in Eq. (4) are typically larger than the positive contribution by the ageostrophic geopotential flux convergence term. In particular, the Reynolds' stress term is often dominant. However, there are a few examples, such as Case 19, that are rather difficult to classify.

Before examining a few of the individual evolutions, it is important to note that a diagnosis can highlight important physical and dynamical processes without explaining why the cyclones of interest develop (Bluestein, 1992). For example, given strong baroclinic conversion associated with the 41 western cyclones examined briefly in Section 4, why does only one produce a strong eastern cyclone (Case 41 of our eastern group)? Although our results suggest that downstream baroclinic development is relevant to about half of the eastern cases, some caveats apply. For instance, the timing of certain western cyclones and subsequent development of the energy

TABLE 1. Dates, positions, and maximum deepening rates of the 20 eastern North Pacific surface cyclones which demonstrate downstream baroclinic development. Particularly good examples are indicated by an asterisk. Dates are listed as year/month/day/UTC hour and positions are given at T0. Included are maximum deepening rates of the western North Pacific cyclones from which a possibly influential eddy energy propagation can be observed (a name denotes the extratropical decay of a tropical cyclone, two rates are listed for primary and secondary cyclones, respectively, and the mid-point time relative to T0 is listed in brackets). Baroclinic conversion (BC) and ageostrophic geopotential flux convergence (GF) contributions (units of per day) to the growth of the energy centres of interest are also shown. For the central energy centre, the positive and negative geopotential flux convergence contributions are shown separately and baroclinic conversion is omitted. Contributions are averaged over 24 h, with the mid-point time relative to T0 listed in brackets.

Case	Onset (T0) Max 24-h Deepening	Cyclone Position (°N/°W)	Max 24-h Deepening (Bergerons)	Max 24-h Upstream Deepening (Ber)	Western 24-h Growth (BC GF)	Central 24–h Growth (+GF -GF)	Eastern 24-h Growth (GF BC)
2	1975/10/27/12	42/151	1.4	0.9 (0 h)	0.8 -0.2 (-12h)	2.1 -0.3 (12h)	0.8 -0.1 (48h)
6	1976/02/16/12	41/161	1.9	0.5 (-48h)	0.6 -1.1 (-36h)	0.3 -2.4 (-24h)	0.6 +0.7 (0 h)
8*	1976/03/15/12	42/149	1.4	0.6 (-36h)	1.7 -1.1 (-24h)	1.0 -0.7 (0 h)	-0.7 +0.5 (24h)
9*	1976/03/20/12	47/156	1.3	0.5 (-24h)	1.2 -0.6 (-36h)	1.6 -1.1 (-12h)	1.4 +0.04 (12h)
10*	1976/10/06/12	31/151	1.2	0.8 (-24h)	1.4 -1.4 (-24h)	1.3 -0.8 (0 h)	-0.4 +0.2 (12h)
12*	1976/11/19/12	42/152	1.6	1.0 (-36h)	3.0 -1.8 (-24h)	1.9 -1.2 (0 h)	2.2 +0.1 (12h)
15*	1977/03/09/12	38/168	1.6	0.8 (0 h)	1.8 -1.1 (-36h)	0.7 -1.1 (-12h)	1.0 +0.5 (12h)
18	1978/02/17/00	39/167	1.3	–	-1.0 +2.1 (-12h)	1.7 -0.6 (0 h)	1.3 +0.5 (24h)
20	1979/02/04/00	58/150	1.2	0.8 (-84h)	1.8 -2.2 (-36h)	1.3 -0.5 (-12h)	-0.8 +0.9 (12h)
21*	1979/10/21/00	46/149	2.1	Tip	3.4 -1.8 (-36h)	1.7 -0.5 (-12h)	1.2 +0.6 (12h)
24*	1980/11/28/12	41/141	1.7	0.8 (-60h)	1.7 -0.8 (-24h)	0.6 -0.8 (0 h)	0.8 +0.2 (12h)
25	1980/12/24/00	34/160	1.4	1.2 (0 h)	0.6 +0.5 (-12h)	2.9 -0.6 (0 h)	0.3 +0.9 (12h)
27*	1981/01/18/00	34/144	1.4	0.9 (-48h)	1.0 -0.9 (-36h)	1.0 -1.6 (-12h)	0.3 +0.6 (0 h)
29	1981/02/18/12	43/148	1.4	1.7 (-12h)	3.0 -2.8 (-36h)	1.3 -1.8 (-24h)	-0.2 +0.3 (0 h)
30	1981/03/06/00	45/147	1.4	1.1 (-24h)	1.1 +0.2 (-36h)	0.8 -1.9 (-12h)	0.9 +0.1 (12h)
32	1983/02/14/12	35/154	1.6	0.9 (12h)	0.3 -1.2 (-12h)	0.5 -2.6 (0 h)	0.9 -0.2 (12h)
33*	1983/03/14/00	32/166	2.1	1.6 (0 h)	0.8 -0.5 (-24h)	0.9 -1.1 (0 h)	2.2 -0.4 (12h)
34	1983/10/23/12	49/164	1.3	0.5/0.5 (-12h)	0.5 +0.4 (-12h)	0.5 -2.5 (0 h)	0.7 +0.3 (12h)
39*	1984/12/02/12	41/159	1.4	0.7/0.8 (-12/0 h)	0.7 -0.1 (-24h)	1.4 -1.4 (-12h)	0.8 +0.02 (12h)
41*	1985/03/09/12	48/163	1.5	1.2 (0 h)	0.9 -0.6 (-24h)	0.9 -0.9 (0 h)	0.7 +0.5 (12h)

TABLE 2. As in Table 1, but for the 21 eastern North Pacific surface cyclones for which downstream baroclinic development is difficult to diagnose. Included are maximum deepening rates of the western North Pacific cyclones which develop in association with the western energy centres of interest (where applicable). In the last two columns, the largest among the Reynolds' stress (RE), horizontal kinetic energy flux convergence (KF), or eddy forcing (EF) growth rates replace what is indicated by the heading when one of these is larger than the corresponding positive contribution by the ageostrophic geopotential flux convergence term (see text). Examples that are difficult to categorize are indicated by an asterisk.

Case	Onset (T0) Max 24-h Deepening	Cyclone Position (°N/°W)	Max 24-h Deepening (Bergerons)	Max 24-h Upstream Deepening (Ber)	Western 24-h Growth (BC GF)	Central 24–h Growth (+GF -GF)	Eastern 24-h Growth (GF BC)
1	1975/10/04/12	44/148	1.6	0.5 (12h)	0.2 +0.2 (-12h)	1.5 -0.4 (12h)	RE +0.8 (24h)
3	1975/11/14/00	39/160	1.5	Ida	1.5 -0.5 (-36h)	RE +0.8 (0 h)	0.2 +0.4 (24h)
4	1975/12/17/12	38/168	1.5	0.6/0.8 (-12/24h)	0.6 +0.3 (-12h)	KF +0.9 (12h)	-0.01 +1.4 (36h)
5	1976/02/07/12	48/153	1.3	1.5 (-36h)	2.9 -1.9 (-24h)	1.8 -0.4 (0 h)	RE +1.5 (24h)
7	1976/03/09/12	35/153	1.3	0.2 (12h)	0.6 +0.7 (-24h)	0.9 -1.2 (0 h)	–
11	1976/11/13/12	44/166	1.6	1.6 (12h)	0.03 -0.4 (-24h)	RE +0.7 (0 h)	0.8 +0.3 (12h)
13	1977/02/01/00	45/153	1.3	–	–	0.9 -1.1 (-12h)	-0.6 +2.0 (12h)
14	1977/02/19/12	40/152	1.5	–	0.5 -1.4 (-24h)	RE +1.7 (0 h)	0.2 +0.8 (24h)
16*	1977/11/16/12	38/150	1.2	0.9 (-12h)	0.04 +0.5 (-12h)	1.2 -0.5 (0 h)	0.5 +0.6 (12h)
17	1977/12/13/12	48/151	1.3	–	–	EF +0.5 (0 h)	0.5 +0.8 (24h)
19*	1978/12/04/00	31/162	1.3	1.5 (-60h)	1.3 -0.8 (-24h)	0.6 -0.8 (0 h)	–
22	1979/11/26/12	30/152	2.3	–	0.1 -0.6 (-12h)	RE +0.9 (0 h)	RE +1.8 (12h)
23*	1979/12/22/12	49/153	1.5	0.8/0.8 (-48/36h)	0.5 -1.1 (-12h)	0.5 -1.0 (0 h)	0.2 +0.2 (12h)
26*	1981/01/12/00	39/135	1.2	0.9 (-12h)	1.5 -1.2 (-24h)	0.9 -1.4 (-12h)	-0.2 +0.6 (12h)
28	1981/02/12/00	33/154	1.3	–	–	RE +1.3 (0 h)	-0.5 +0.8 (24h)
31	1981/12/16/12	36/169	1.5	1.9 (-84h)	-0.01 -0.7 (-12h)	RE +0.9 (0 h)	0.6 +0.6 (12h)
35	1983/12/24/12	25/164	1.6	0.8/0.9 (-36h)	1.5 -1.4 (-36h)	RE +1.5 (-24h)	1.6 -0.1 (0 h)
36	1984/03/27/00	44/148	1.2	0.6 (-24h)	0.5 -0.5 (-24h)	KF +0.9 (-12h)	-0.6 +0.7 (0 h)
37	1984/10/11/12	45/149	1.6	–	–	EF +0.6 (-12h)	-0.2 +0.4 (12h)
38	1984/10/24/00	53/152	1.3	1.0/0.6 (-96/12h)	2.2 -2.0 (-48h)	1.0 -0.4 (-24h)	RE +1.3 (0 h)
40	1985/01/27/12	42/164	1.3	1.2 (12h)	-0.9 +0.02 (-12h)	RE +0.8 (0 h)	-0.1 +0.6 (12h)

centres downstream appear to be early relative to T0 in Cases 6, 20, and 29, and late in Cases 12, 18, 25, and 34. For these examples, the existence of a western cyclone may be of minor importance to the development of the corresponding eastern cyclone, particularly among the evolutions that are delayed.

6 Individual evolutions

We might presume that all 41 eastern cyclones depend directly on an eastern trough for their development. The previous section suggests that only about half of these cyclones have a direct dependence on an entire wavetrain of troughs

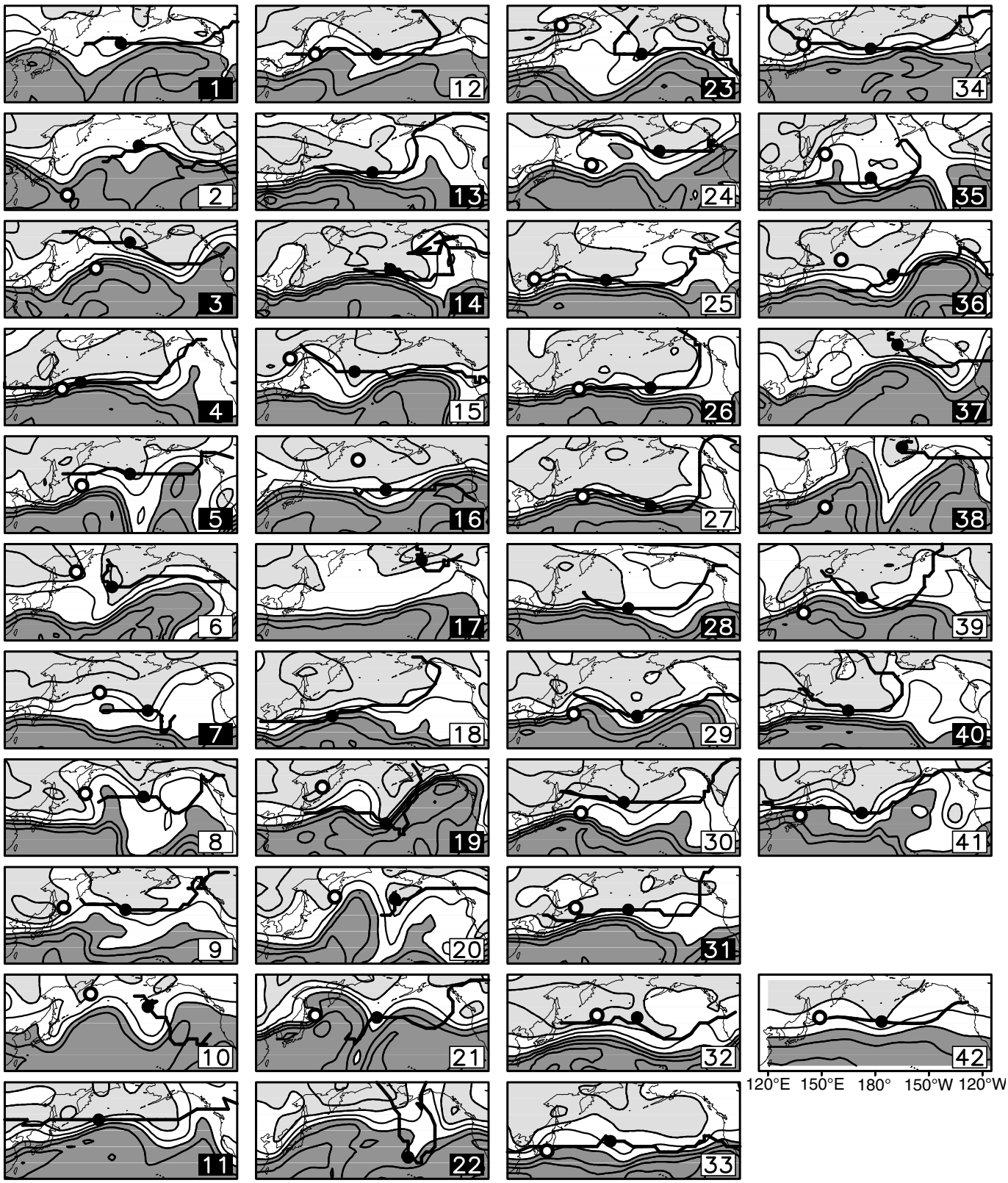

Fig. 5 Tropopause potential temperature for the 41 eastern cyclones at T0-24 h. Tropopause depression tracks are shown with a filled circle to indicate position. The contour interval is 15 K, with values above 335 K shaded darkly and below 305 K shaded lightly. Numbered labels correspond to the 20 events of Table 1 (2, 6, 8, etc.) and the 21 events of Table 2 (1, 3, 4, etc.); also shown is a composite (42). Open circles denote western North Pacific surface cyclones that appear to be upstream sources of eddy energy (see text). The domain shown extends from 20°N to 65°N.

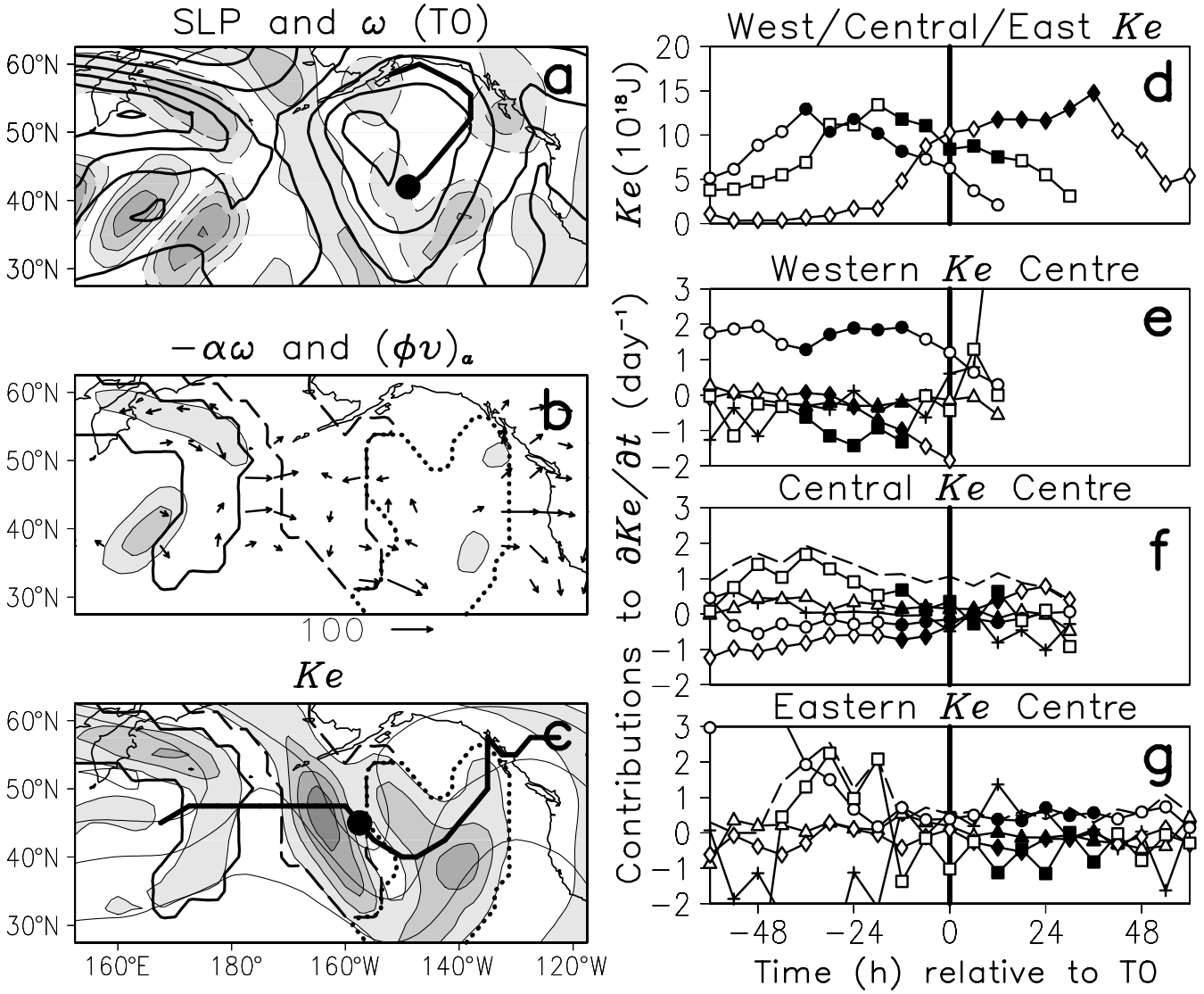

Fig. 6 A summary of local eddy energetics for Case 8 (see text). Panels a–c show fields at 12:00 UTC 15 March 1976 (T0). a) SLP and 500-hPa vertical velocity. Contour intervals are somewhat larger than was the case for the composites (8 h Pa and 0.15 Pa s^{-1}, respectively). b) The vertically integrated baroclinic conversion term (35-W m^{-2} intervals) and ageostrophic geopotential flux (vectors less than 20 MW m^{-1} are omitted). c) Vertically integrated eddy kinetic energy (1-MJ m^{-2} intervals) and 500-hPa height (20-dam intervals). The surface cyclone and tropopause depression tracks are shown in (a) and (c), respectively. The western, central, and eastern energy centres are bounded by solid, dashed, and dotted contours in (b) and (c). The evolution of these centres is denoted by circles, squares, and diamonds, respectively in (d). Panels (e)–(g) depict contributions to the growth of these centres by baroclinic conversion (circles), ageostrophic geopotential flux convergence (squares) and its positive contribution (dashed lines in panels (f) and (g); see text), quasi-Lagrangian flux convergence (triangles), Reynolds' stress (diamonds), and all remaining contributions to the tendency of eddy kinetic energy (crosses). The filled marks in (d)–(g) indicate 24-h averaging periods over which budget summaries are computed (see text).

and ridges. To understand variations from case to case better, a closer examination of a few eastern cyclones is given in this section. Before proceeding, however, we qualitatively assess the presence of wavetrains for each of the 41 eastern cyclones in Fig. 5. Features of the tropopause flow are shown at T0-24 h when the composite dispersion of energy across an upstream ridge toward a predecessor trough is most evident (Fig. 2d). Large-scale features include the North Pacific jet stream (a strong meridional gradient) and troughs and ridges (potential temperature undulations). Tropopause depressions are generally found poleward of the strongest gradients and near a local minimum of potential temperature. They translate roughly with the large-scale flow. There is the suggestion of Group A flows being more undular and Group B flows being more zonal. Perhaps most striking, however, is the variety of flows sampled by these 41 events.

Although each individual evolution may be relevant, for brevity we examine in sequence Cases 8, 38, and 41 (where case numbers are taken from Fig. 5 and Tables 1 and 2). These reveal more of the case-to-case variability among the larger sample of cyclones and they suffice to illustrate our

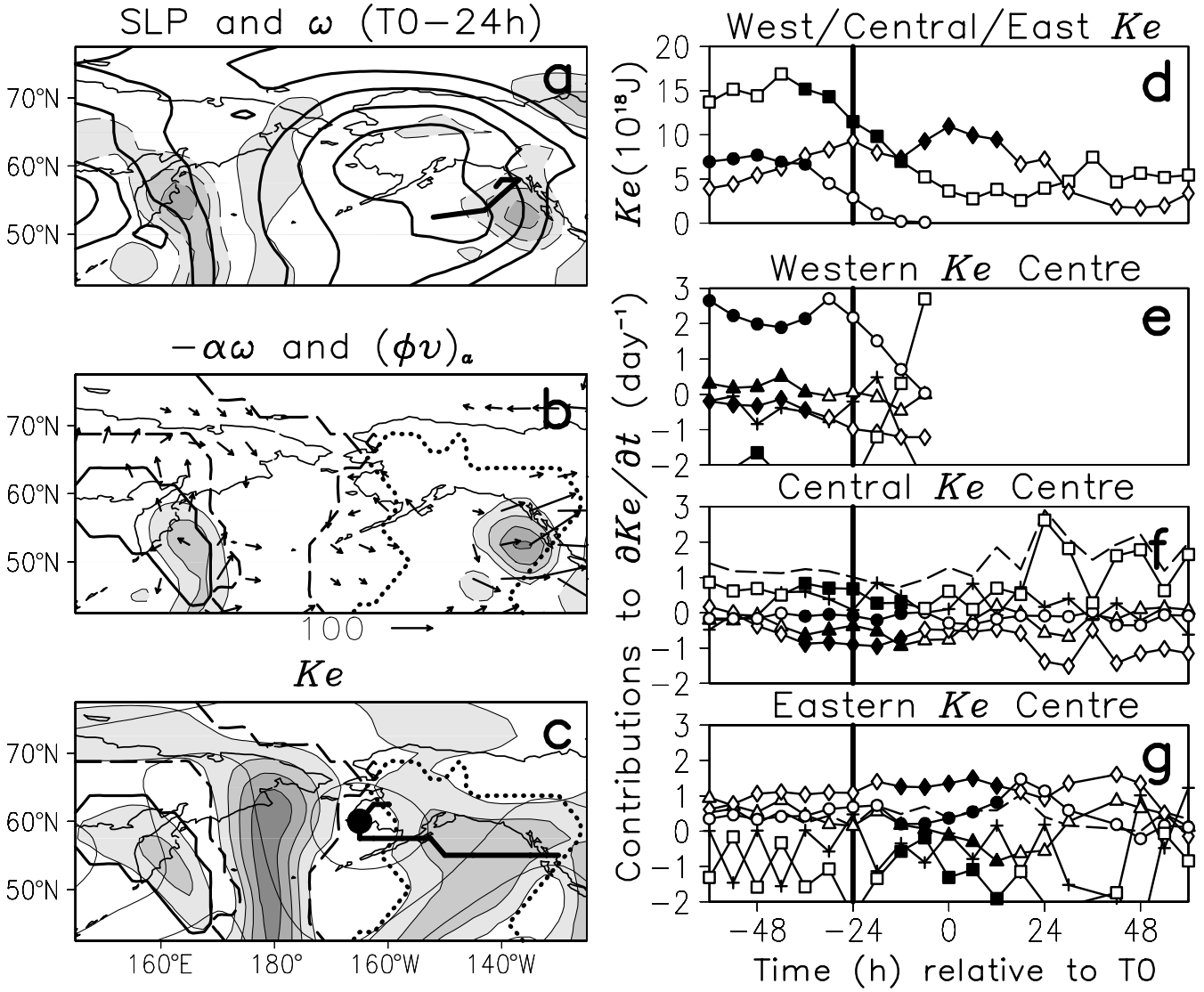

Fig. 7 A summary of local energetics as in Fig. 6, but for Case 38 (see text) at 00:00 UTC 23 October 1984 (T0-24 h; the absence of an eastern surface cyclone position in panel (a) is due to its formation at T0).

application of the criteria of Section 5. While Cases 8 and 41 are both good examples satisfying all three criteria, Case 38 is one that does not satisfy the final criterion. Local energetics are summarized with reference to figures such as Fig. 6. We choose a representative time to depict surface cyclones, mid-level vertical motion, and selected energy budget terms. The three eddy energy centres are bounded by vertically integrated energy contours (e.g., Fig. 6c). We also depict the evolution of energy within these centres and the contributions to their growth (e.g., Fig. 6d–6g). The 24–h budget summaries for each centre are indicated by filled marks. Note that case-to-case variability generally prohibits choosing 24–h intervals at the same time relative to T0. Each interval has been selected to emphasize the energy dispersing between adjacent energy centres.

From Fig. 5, a strong potential temperature gradient to the south is absent in Case 8, and the initially negatively tilted (north-west to south-east) trough elongates southward, with the tropopause depression becoming an isolated feature. Immediately south of a decaying cyclone (Fig. 6a), the strongly deepening cyclone of interest forms. Downstream baroclinic development in Case 8 is initiated by the trough to the west (Figs 5 and 6c). Associated with this upstream trough at T0 is a decaying western cyclone (Fig. 6a) with baroclinic conversion by warm ascent to the north (Fig. 6b). The western energy centre has peaked in amplitude 36 h earlier (Fig. 6d), but energy is still dispersing toward the central energy centre. The central energy centre does not have a baroclinic source of energy, although energy nevertheless disperses downstream. Similarly, the eastern centre both receives energy from upstream and disperses energy farther downstream.

If we focus on the selected 24–h summary periods for the three energy centres (the filled marks in Figs 6e–6g), the western centre is characterized by large baroclinic conversion and

ageostrophic geopotential flux divergence (Figs. 6e). The central energy centre is subsequently maintained by a geopotential flux convergence and to a lesser extent by an advective flux convergence. Moreover, we show that positive contributions from the geopotential flux convergence term (the dashed line) are dominant (Fig. 6f). The eastern centre grows partly by baroclinic conversion following T0 (Fig. 6g). Although there is a strong net divergence of the ageostrophic geopotential flux, the central energy centre appears to act as a source nevertheless (Fig. 6b). Consistent with this, we find that the positive contribution by geopotential flux convergence (the dashed line) is not at all negligible. It is second only to baroclinic conversion. Thus, it appears that the energy dispersing from the western cyclone influences the eastern centre and the development of the eastern cyclone.

Case 38 is an example for which the third criterion is not satisfied. The tropopause depression is initially associated with a decaying predecessor cyclone in the Gulf of Alaska (Figs 7a and 7c). The eastern surface cyclone of interest develops entirely within this region, while the tropopause depression eventually tracks to the east. Initially upstream, two western cyclones (a primary and secondary pair which are partly shown in Fig. 7a west and south of the Kamchatka peninsula) are associated with baroclinic conversion and a dispersion of energy toward the central energy centre (Fig. 7b). However, a dispersive flux of eddy energy that might be expected to occur toward the eastern centre is very weak at T0-24 h, and at any time, an ageostrophic geopotential flux convergence which contributes to the growth of the eastern centre is lacking (not shown). Instead, the eastern centre grows mainly in association with Reynolds' stresses and by baroclinic conversion in warm ascent (Fig. 7g). Energy dispersing farther downstream contributes to the decay of this centre. Hence, it seems unlikely that energy originating from the western cyclones influences the eastern cyclone.

We note in passing that the ageostrophic geopotential flux convergence and residual terms are sometimes dominated by a semi-diurnal signal (e.g., Fig. 6g and Fig. 7g). We associate these oscillations with the semi-diurnal tide, whose tropospheric effects were first studied using radiosonde data (Wallace and Hartranft, 1969). To confirm that these are also resolved here, we have employed the simple model of Whiteman and Bian (1996) and found that the oscillations can be partly removed (not shown). Other studies also confirm that gridded analyses are able to resolve the semi-diurnal tide (Hsu and Hoskins, 1989).

The final example is that of Case 41, which is another good example of downstream baroclinic development. The tropopause depression is initially unassociated with a predecessor cyclone and becomes negatively tilted after T0 (not shown). Associated with a trough to the west, a western cyclone develops rapidly and downstream baroclinic development then follows. At T0, the western cyclone is well developed (Fig. 8a), and a large baroclinic conversion by warm ascent is occurring. The western energy centre has peaked in amplitude (Fig. 8d), and energy is dispersing toward the growing central energy centre. The eastern centre is weaker and is collocated with the eastern surface cyclone.

Based on the selected 24-h summary periods, the western centre grows primarily by baroclinic conversion and decays by energy dispersion (Fig. 8e). Subsequent growth of the central centre occurs by baroclinic conversion and quasi-Lagrangian flux convergence. Ageostrophic geopotential fluxes are apparent between the adjacent energy centres at T0, and are both strongly convergent and divergent within this centre (not shown). Though their net effect may be negligible (Fig. 8f), during this 24-h period the positive contributions by this term (the dashed line) are clearly dominant. Following T0, the eastern centre grows mainly as a result of energy dispersing toward it, as well as an in situ baroclinic conversion. As with Case 8, it appears that the energy dispersing from the western cyclone influences the development of the eastern cyclone.

Conclusions

For the 41 eastern North Pacific cyclones examined here, we find that downstream baroclinic development represents their composite evolution fairly well (Fig. 2). Case-to-case variability is large, however, with downstream baroclinic development offering a good description of about half of these events (Fig. 4a). A composite evolution of vertically integrated eddy energy shows evidence of downstream development. About 45° longitude upstream, an SLP minimum and upward motion are found 24 h before the eastern cyclones begin to deepen.

Composite features are suggestive of predecessor cyclones that initiate downstream baroclinic development (Orlanski and Sheldon, 1995), but they do not appear robust enough to be present in all cases. However, supporting evidence that downstream baroclinic development is generally relevant to our eastern group was provided by a composite comparison with 41 similarly intensifying cyclones in the western North Pacific. Much stronger baroclinic conversion is associated with the western group, while baroclinic conversion to the west and downstream dispersion exists prior to the development of the eastern cases.

To examine each case, we have subjectively isolated the two eddy energy centres bracketing the eastern trough associated with each eastern surface cyclone. Where possible, we have also isolated the western energy centre immediately upstream, and have measured contributions to the growth of these three centres. This revealed that events comparing favourably to the proposed evolution constitute about half of our cases. What distinguishes these events is that energy initially disperses from the western energy centre, and this is followed by successive positive contributions by ageostrophic geopotential flux convergence to the growth of the two energy centres downstream.

Favourable cases are almost always initiated in the western North Pacific by an interacting trough and surface cyclone (or a decaying tropical cyclone). A variety of evolutions follow, not all of which are synchronized with the onset of rapid deepening. Baroclinic conversion occurs upstream by warm ascent, augmented in some cases by energy propagating from farther upstream. Energy disperses from the western energy centre toward the centre upstream of the eastern trough. This

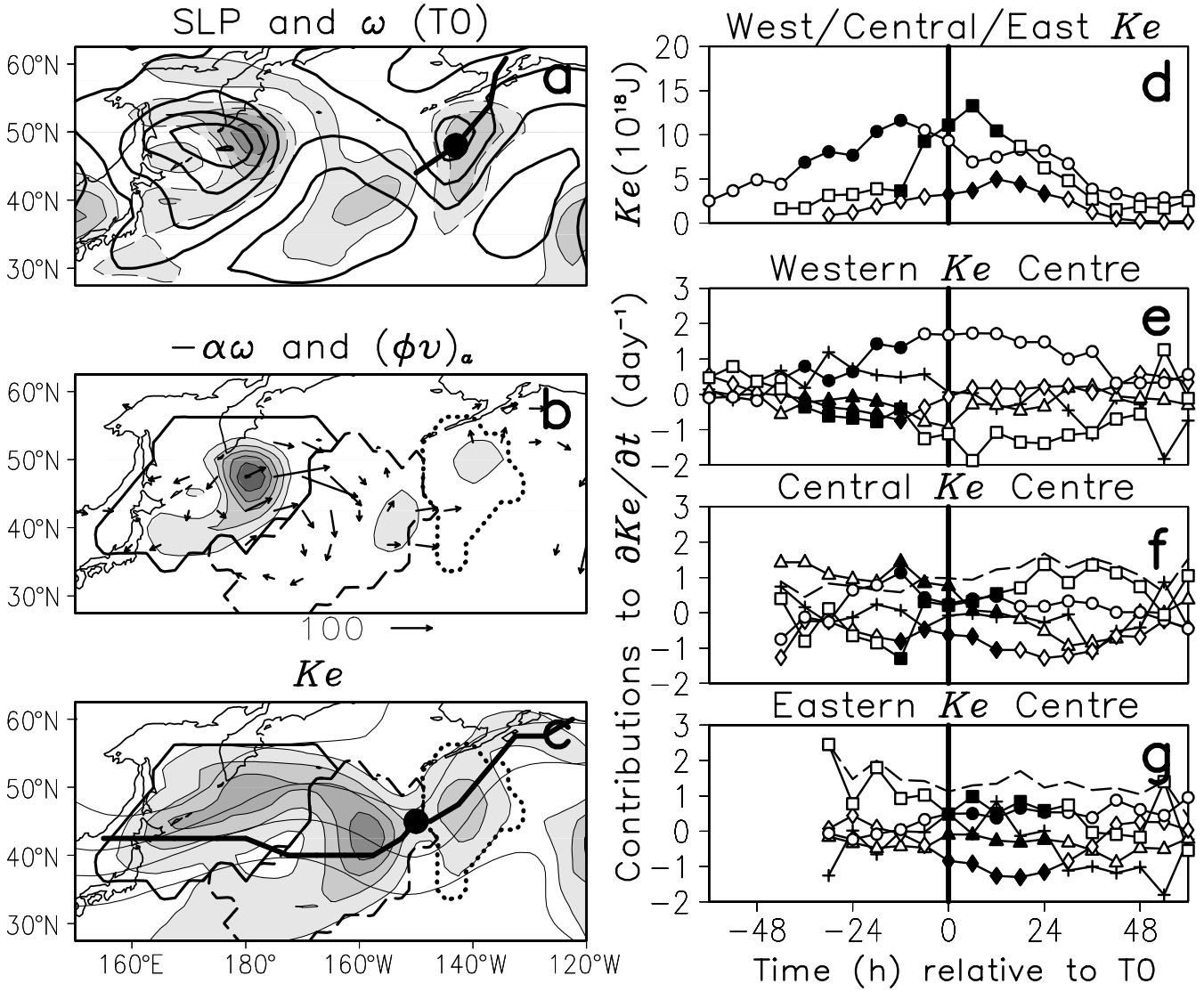

Fig. 8 A summary of local energetics as in Fig. 6, but for Case 41 (see text) at 12:00 UTC 9 March 1985 (T0).

intermediate energy centre also benefits from non-negligible contributions by quasi-Lagrangian flux convergence or Reynolds' stresses, though these are often negative. Subsequently, a dispersion occurs toward the energy centre collocated with the eastern surface cyclone. In some cases, this occurs at the same time as the dispersion from the western energy centre. The growth of the eastern energy centre is subsequently defined in part by an ageostrophic geopotential flux convergence. Other local contributions to the eastern cyclone include baroclinic conversion, Reynolds' stresses, which can be positive or negative, and contributions by the remaining terms which are generally negative.

Aspects of downstream baroclinic development are apparent in most of the unfavourable cases as well. (This is especially true of Cases 5, 16, 22, 31, 35, and 36, for which all three energy centres exist and show evidence of a sequential evolution.) Some cases also include the presence of a developing cyclone in the western North Pacific, or energy dispersing between at least two of the energy centres of interest. Nevertheless, most of these evolutions are interrupted, typically at the upstream centre, by a local contribution which is dominant (possibly with the exception of baroclinic conversion). The relative unimportance of energy dispersion in these cases implies that an upstream influence is probably quite weak. However, included among these cases are a few that are difficult to categorize.

A majority of the strongly deepening eastern North Pacific cyclones from ten cold seasons have been examined in this study. We have thus characterized individually many of the events considered by previous climatological studies (e.g., Roebber, 1984; Gyakum et al., 1989). Our results lend weight to a dynamical interpretation of the local maximum in strong cold-season cyclogenesis in the eastern North Pacific (cf. Roebber, 1984), though we cannot overlook the possibility

that this climatological feature might be partly an artefact of poor observations. We have implicitly assumed that an eddy energy diagnosis resolves downstream development and other relevant processes, though this assumption could be addressed using a different diagnosis (Nielsen-Gammon and Lefevre, 1996; Takaya and Nakamura, 2001). Following this approach, however, it would remain unclear precisely how much of the intensification of the cyclones we have examined results from an upstream influence. In a subsequent case study, we intend to report on a complementary diagnosis and numerical simulation to validate the diagnosis of Case 15, one of the better examples of downstream baroclinic development.

Acknowledgements

Numerous suggestions by the three anonymous reviewers helped to strengthen our presentation and these are gratefully acknowledged. This research was sponsored by the Natural Sciences and Engineering Research Council, Environment Canada, and the Canadian Foundation for Climate and Atmospheric Sciences. Gridded data were obtained through the Climate Diagnostics Center at Boulder, Colorado. Data visualization and feature tracking were facilitated by the GrADS software obtained from the Institute of Global Environment and Society at Calverton, Maryland.

References

BLUESTEIN, H. B. 1992. *Synoptic-Dynamic Meteorology in Midlatitudes*, Vol. I, *Principals of Kinematics and Dynamics*. Oxford University Press, New York, New York, 431 pp.

CHANG, E. K. M. 1993. Downstream development of baroclinic waves as inferred from regression analysis. *J. Atmos. Sci.* **50**: 2038–2053.

———. 1999. Characteristics of wave packets in the upper troposphere. Part II: Seasonal and hemispheric variations. *J. Atmos. Sci.* **56**: 1729–1747.

———. 2000. Wave packets and life cycles of troughs in the upper troposphere: Examples from the southern hemisphere summer season of 1984/85. *Mon. Weather Rev.* **128**: 25–50.

——— and I. ORLANSKI. 1993. On the dynamics of a storm track. *J. Atmos. Sci.* **50**: 999–1015.

——— and ———. 1994. On energy flux and group velocity of waves in baroclinic flows. *J. Atmos. Sci.* **51**: 3823–3828.

——— and D. B. YU. 1999. Characteristics of wave packets in the upper troposphere. Part I: Northern hemisphere winter. *J. Atmos. Sci.* **56**: 1708–1728.

CORFIDI, S. F. and K. E. COMBA. 1989. The meteorological operations division of the National Meteorological Center. *Weather Forecast.* **4**: 343–366.

GYAKUM, J. R.; ANDERSON, R. H. GRUMM and E. L. GRUNER. 1989. North Pacific cold-season surface cyclone activity: 1975–1983. *Mon. Weather Rev.* **117**: 1141–1155.

——— and R. E. STEWART. 1996. A multiscale analysis of a case of slow growth/rapid cyclogenesis during CASP II. ATMOSPHERE–OCEAN, **34**: 17–50.

——— and R. E. DANIELSON. 2000. Analysis of meteorological precursors to ordinary and explosive cyclogenesis in the western North Pacific. *Mon. Weather Rev.* **128**: 851–863.

HAKIM, G. J. 2003. Developing wave packets in the North Pacific storm track. *Mon. Weather Rev.* **131**: 2824–2837.

HOSKINS, B. J.; M. E. MCINTYRE and A. W. ROBERTSON. 1985. On the use and significance of isentropic potential vorticity maps. *Q. J. R. Meteorol. Soc.* **111**: 877–946.

——— and P. J. VALDES. 1990. On the existence of storm-tracks. *J. Atmos. Sci.* **47**: 1854–1864.

HOVMÖLLER, E. 1949. The trough and ridge diagram. *Tellus,* **1**: 62–66.

HSU, H.-H. and B. J. HOSKINS. 1989. Tidal fluctuations as seen in ECMWF data. *Q. J. R. Meteorol. Soc.* **115**: 247–264.

KALNAY, E.; M. KANAMITSU, R. KISTLER, W. COLLINS, D. DEAVEN, L. GANDIN, M. IREDELL, S. SAHA, G. WHITE, J. WOOLLEN, Y. ZHU, A. LEETMAA, B. REYNOLDS, M. CHELLIAH, W. EBISUZAKI, W. HIGGINS, J. JANOWIAK, K. C. MO, C. ROPELEWSKI, J. WANG, R. JENNE and D. JOSEPH. 1996. The NCEP/NCAR 40-year reanalysis project. *Bull. Am. Meteorol. Soc.* **77**: 437–471.

LACKMANN, G. M., D. KEYSER and L. F. BOSART. 1999. Energetics of an intensifying jet streak during the Experiment on Rapidly Intensifying Cyclones over the Atlantic (ERICA). *Mon. Weather Rev.* **127**: 2777–2795.

LEE, S. and I. M. HELD. 1993. Baroclinic wave packets in models and observations. *J. Atmos. Sci.* **50**: 1413–1428.

MAGNUSDOTTIR, G. and P. H. HAYNES. 1996. Wave activity diagnostics applied to baroclinic wave life cycles. *J. Atmos. Sci.* **53**: 2317–2353.

MARTIN, J. E.; R. D. GRAUMAN and N. MARSILI. 2001. Surface cyclolysis in the North Pacific Ocean. Part I: A synoptic climatology. *Mon. Weather Rev.* **129**: 748–765.

MORGAN, M. C. and J. W. NIELSEN-GAMMON. 1998. Using tropopause maps to diagnose midlatitude weather systems. *Mon. Weather Rev.* **126**: 2555–2579.

MURTY, T. S.; G. A. MCBEAN and B. MCKEE. 1983. Explosive cyclogenesis over the northeast Pacific Ocean. *Mon. Weather Rev.* **111**: 1131–1135.

NAMIAS, J. and P. F. CLAPP. 1944. Studies of the motion and development of long waves in the westerlies. *J. Meteorol.* **1**: 57–77.

NIELSEN-GAMMON, J. W. 1995. Dynamical conceptual models of upper-level mobile trough formation: Comparison and application. *Tellus,* **47**A: 705–721.

——— and R. J. LEFEVRE. 1996. Piecewise tendency diagnosis of dynamical processes governing the development of an upper-tropospheric mobile trough. *J. Atmos. Sci.* **53**: 3120–3142.

ORLANSKI, I. and J. KATZFEY. 1991. The life cycle of a cyclone wave in the southern hemisphere. Part I: Eddy energy budget. *J. Atmos. Sci.* **48**: 1972–1998.

——— and J. P. SHELDON. 1993. A case of downstream baroclinic development over western North America. *Mon. Weather Rev.* **121**: 2929–2950.

——— and ———. 1995. Stages in the energetics of baroclinic systems. *Tellus,* **47A**: 605–628.

PETTERSSEN, S. and S. J. SMEBYE. 1971. On the development of extratropical cyclones. *Q. J. R. Meteorol. Soc.* **97**: 457–482.

REED, R. J. and M. D. ALBRIGHT. 1986. A case study of explosive cyclogenesis in the eastern North Pacific. *Mon. Weather Rev.* **114**: 2297–2319.

ROEBBER, P. J. 1984. Statistical analysis and updated climatology of explosive cyclones. *Mon. Weather Rev.* **112**: 1577–1589.

SANDERS, F. and J. R. GYAKUM. 1980. Synoptic-dynamic climatology of the "Bomb''. *Mon. Weather Rev.* **108**: 1589–1606.

SIMMONS, A. J. and B. J. HOSKINS. 1979. The downstream and upstream development of unstable baroclinic waves. *J. Atmos. Sci.* **36**: 1239–1254.

TAKAYA, K. and H. NAKAMURA. 2001. A formulation of a phase-independent wave-activity flux for stationary and migratory quasigeostrophic eddies on a zonally varying basic flow. *J. Atmos. Sci.* **58**: 608–627.

THORNCROFT, C. D.; B. J. HOSKINS and M. E. MCINTYRE. 1993. Two paradigms of baroclinic-wave life-cycle behaviour. *Q. J. R. Meteorol. Soc.* **119**: 17–55.

WALLACE, J. M. and F. R. HARTRANFT. 1969. Diurnal wind variations, surface to 30 kilometers. *Mon. Weather Rev.* **97**: 446–455.

———; G.-H. LIM and M. L. BLACKMON. 1988. Relationship between cyclone tracks, anticyclone tracks and baroclinic waveguides. *J. Atmos. Sci.* **45**: 439–462.

WHITEMAN, C. D. and X. BIAN. 1996. Solar semidiurnal tides in the troposphere: Detection by radar profilers. *Bull. Am. Meteorol. Soc.* **77**: 529–542.